ACS Sustainable Chemistry & Engineering

Research Article

Cite This: ACS Sustainable Chem. Eng. XXXX, XXX, XXX−XXX

pubs.acs.org/journal/ascecg

Nanocellulose-Reinforced Organo-Inorganic Nanocomposite for Synergistic and Affordable Defluoridation of Water and an Evaluation of Its Sustainability Metrics

Sritama Mukherjee,[†,‡] Haritha Ramireddy,[†] Avijit Baidya,[†] A. K. Amala,[†] Chennu Sudhakar,[†] Biswajit Mondal,[†] Ligy Philip,[‡] and Thalappil Pradeep*[,†]

[†]DST Unit of Nanoscience (DST UNS) and Thematic Unit of Excellence (TUE), Department of Chemistry and [‡]EWRE Division, Department of Civil Engineering, Indian Institute of Technology Madras, Chennai 600036, India

Supporting Information

ABSTRACT: Fluoride (F^-) is one of the common naturally occurring anions present in groundwater worldwide that may be beneficial or detrimental depending on the total amount ingested and the duration of exposure. Among all the remediation techniques, adsorption using nanomaterials shows superior efficiency and the process can be eco-friendly and economical. We report cellulose nanofiber-polyaniline (PANI)-templated ferrihydrite nanocomposite synthesized by a green one-pot process where the iron precursor not only acts as an oxidant for the polymerization of aniline to give emaraldine base−emaraldine salt (EB−ES) form of PANI but also forms 2-line ferrihydrite (FeOOH) nanoparticles in situ. These nanoparticles get embedded into the cellulose−PANI blend to give a granular nanocomposite having double action sites for adsorption and robustness which also prevent nanoparticle leaching. Doped PANI and FeOOH act as synergistic adsorption sites for F^- removal which results in an enhanced uptake capacity. The materials' adsorption mechanism and removal performance have been evaluated by diverse analytical techniques. The investigations led to the conclusion that the material is suitable to be used as adsorption media in the form of simple cartridges for gravity-fed water purification. In addition, the impact of such materials on the environment has been assessed by evaluating the relevant sustainability metrics and socio-economic parameters.

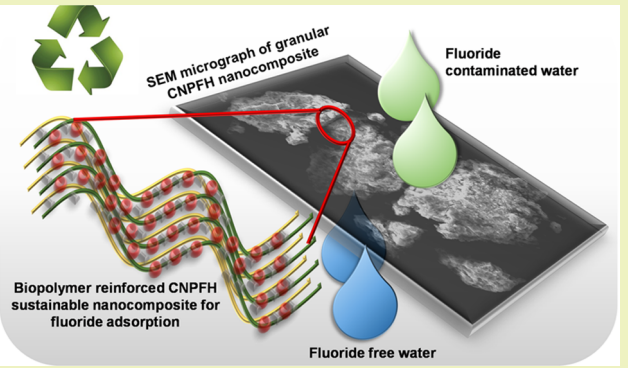

KEYWORDS: *fluoride, cellulose nanofiber, polyaniline, ferrihydrite, synergy, sustainability metrics*

1. INTRODUCTION

Fluorine is the lightest halogen and the most electronegative element of the periodic table. It ranks 13th in terrestrial abundance and 625 mg/kg of it can be found in the earth's crust.[1] In nature, it exists as fluoride anion (F^-) and occurs mainly as sedimentary rocks like fluorspar, apatite, and so forth.[2] These fluoride minerals are mostly insoluble in water, unless factors like high alkalinity, temperature, and low fluoride and high bicarbonate concentrations in the water medium cause its mobilization, thereby resulting in fluoride contamination.[1,3] The hydrogeochemical factors give rise to natural F^- in groundwater in the range of 0.5−50 ppm, keeping the latter's color, smell, and taste intact. Although a concentration up to 1−1.5 mg/L is the requirement for good dental health, prolonged exposure to water consisting F^- in the range of 1.5−4 and 4−10 mg/L is known to cause dental and skeletal fluorosis, respectively.[2,4,5] Fluorosis is known to affect over 200 million people, from about 25 countries across the globe, making F^- one of the deadliest inorganic pollutants of natural origin in groundwater.[6−8] The risk of fluorosis because of human consumption of such water is faced by many countries, notably India, Sri Lanka, China, Chile, Mexico, and Hungary, the Rift Valley countries in East Africa, Turkey, and parts of South Africa.[7,9] Solution for F^- contamination is suggested to be an affordable removal method with simplicity in design and operation.

Defluoridation can be carried out at household and community levels.[6] Conventionally, coagulation and precipitation on activated alumina, alum, and calcium hydroxide have been widely employed which results in an unpleasant taste for the resultant water and increase in the residual ion concentration.[10−15] Other methods like membrane filtration, reverse osmosis, electrocoagulation, dialysis, and ion exchange are efficient but expensive and cumbersome, and also require high maintenance.[16−21] Adsorption is a widely used process which is economical as well as simple to use.[6,22] It gives

Received: August 16, 2019
Revised: October 24, 2019

DOI: 10.1021/acssuschemeng.9b04822
ACS Sustainable Chem. Eng. XXXX, XXX, XXX−XXX

Scheme 1. Illustration of CNPFH used For Fluoride Removal from Water

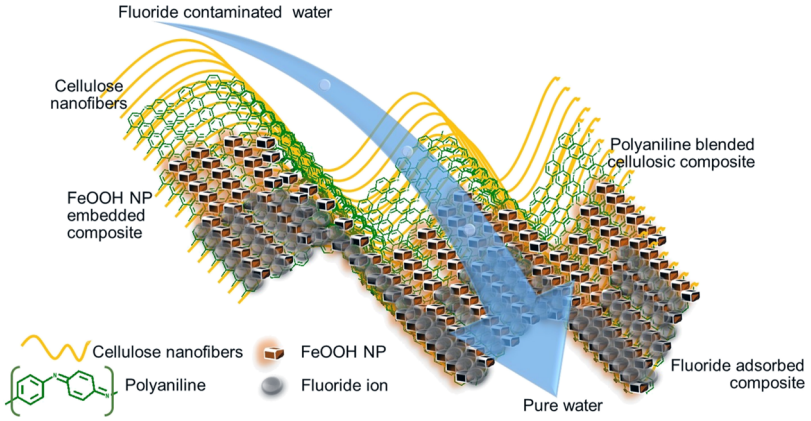

satisfactory results with less operation time by means of mechanisms like external mass transfer, surface adsorption, and intraparticle diffusion. Many low cost adsorbents have also been employed for fluoride removal like alumina, red mud, clays, fly ash, activated carbon, calcite, brick powder, activated coconut-shell, oxide ores, and bone char, which exhibit varying uptake capacities.[3,6] Activated alumina is popular amongst other adsorbents because of its high surface area, which induced greater uptake while maintaining its structural stability without shrinkage, swelling, or disintegration in water.[2,23,24] Other metal oxide- and hydroxide-based adsorbents prepared in micro and nanoforms include modified ferric oxide/hydroxide, hydroxyapatite, magnesium, zirconium, and cerium-modified materials, titanium-derived adsorbent, schwertmannite, zeolite, and so forth; all of them show higher uptake and selectivity toward fluoride.[21,25−30] Biopolymer-derived adsorbents like chitosan, chitosan derivatives, and metal (Mg, Al, Fe, Zr, Ce, La, and Nd) impregnated chitosan have been thoroughly studied giving adsorption capacities ranging from 1.39 mg/g for raw chitosan to 44.4 mg/g for silica-coated chitosan.[31,32] Although, chitosan is environmentally friendly, it is derived from crustacean shells and is a less sustainable option as compared to plant sources. Its polycrystalline nature reduces uptake capacities as adsorption takes place only on the amorphous region available on the surface. On the other hand, nanocellulose, derived from cotton or wood pulp, having hydrophilic surface chemistry, high strength, chemical inertness, and high surface area is a promising material to be used as a matrix for adsorbent synthesis.[33] Cellulose nanofibers (CNFs), typically in the range of 2−20 nm in diameter and 1−100 μm in fiber length and is exposed with hydroxyl groups in the process of production.[34,35] Polymer-based nanocomposites have become a prominent area of research in the field of water purification because of the advantages like film forming ability, dimensional variability, and availability of various tunable functional groups. Polyaniline (PANI), polypyrrole (PPy), polythiophene, and their derivatives/analogues, have gained popularity as chemical adsorbents because of their facile synthesis, porous structure, good electrorheological property, and insolubility in water.[36] With the advancement in nanoscience and nanotechnology, it is now easy to engineer the polymeric composites with specific nanoparticles to enhance efficiency, as per the requirement.

In this work, a cellulose nanofiber-PANI-templated ferrihydrite (CNPFH) nanocomposite was prepared by a one pot synthesis process via an in situ polymerization method. The simple synthesis yielded a sustainable composite which was used for F^- removal from water by means of adsorption. This is an eco-friendly adsorbent with high F^- uptake capacity. Iron oxyhydroxide (FeOOH) is already reported as an efficient arsenic (As) remover but a poor performer in the case of F^-.[29,37] PANI shows unique, yet simple doping/dedoping and redox chemistry, and it is cost-effective and nonhazardous in pure form.[38] It also has been reported as a F^- remover but with a meager uptake capacity of 0.8 mg/g.[35] Here, FeOOH and PANI were blended together and trapped in the CNF matrix to get a robust composite for an improved synergistic performance toward F^- removal. Both of these entities together not only give a greater number of surface active sites but also enhance the kinetics of adsorption. Our previous studies have brought out synergy in the performance of several nanostructures in water adsorption (Scheme 1).

2. EXPERIMENTAL SECTION

2.1. Materials. Native CNF gel (2.8 wt %) was purchased from BioPlus. Ferric chloride hexahydrate ($FeCl_3{\cdot}6H_2O$) and NaOH were purchased from RANKEM Glasswares and Chemicals Pvt. Ltd., India. Aniline (extrapure, AR 99.5%) was purchased from SRL Pvt. Ltd. Sodium fluoride Emparta was purchased from Merck. Deionized (DI) water was used throughout the experiments unless otherwise mentioned.

2.2. Methods: Synthesis of the CNPFH Nanocomposite. Aniline (2 mL) was taken in 60 mL DI water and was kept stirring for 30 min. CNF slurry (5 g) was mixed in 10 mL of water which was then added to the aniline solution. After another 30 min stirring, 1.5 g of $FeCl_3{\cdot}6H_2O$ was added to the reaction mixture. The resultant pH of the mixture was about 1.2 which was adjusted to 4 by dropwise addition of 2 M NaOH. The resultant slurry was stirred for 12 h, followed by filtration and washing with DI water. The precipitate collected was dried at 50 °C to get shiny black chunks. The chunks were crushed mechanically and sieved to get the granular adsorbent media. The product obtained was about 1.8 g.

2.3. Batch Adsorption Studies. In a typical batch adsorption experiment, 25 mg of the granular media were shaken with 100 mL of F^- spiked distilled water of 10 mg/L concentration in a 250 mL polypropylene vessel. The vessels were agitated at 200 rpm in a thermostatic shaker at room temperature (25 ± 2 °C). The water sample was collected to measure the leftover F^- concentration in treated water as a function of time and dosage, using a fluoride-ion-selective electrode (ISE). The maximum uptake of F^- (q_e) by CNPFH was calculated using the eq S1.

2.4. pH Effect. To know the pH effect on F^- adsorption, 25 mg of granular media were added to 25 mL of F^- spiked water, adjusted to the required pH by 1 M HCl/1 M NaOH and shaken for 3 h. The treated water sample was analyzed by ISE.

DOI: 10.1021/acssuschemeng.9b04822
ACS Sustainable Chem. Eng. XXXX, XXX, XXX−XXX

2.5. Interfering Ions. To understand the effect of interfering ions on As adsorption, the ions of interest which generally exist in ground water, like calcium (Ca^{2+}), magnesium (Mg^{2+}), potassium (K^{+}), sodium (Na^{+}), chloride (Cl^{-}), carbonate (CO_3^{2-}), bicarbonate (HCO_3^{-}), nitrate (NO_3^{-}), silicate (SiO_3^{2-}), and sulfate (SO_4^{2-}) were spiked in 25 mL of distilled water in separate conical flasks, with concentrations relevant to ground water. This water was treated with 25 mg of CNPFH for 3 h and ISE measurements were conducted. The relevant water quality parameters are listed (Table S2, Supporting Information).

3. INSTRUMENTATION

Transmission electron microscopy (TEM) and high-resolution TEM (HRTEM) were performed at an accelerating voltage of 200 kV on a JEOL 3010, 300 kV instrument equipped with a UHR polepiece. The accelerating voltage was kept low to ensure that the beam-induced damage on the material was low. The samples for HRTEM were prepared as the dispersions which were drop casted on carbon-coated copper grids and allowed to dry under ambient conditions. Surface morphology, elemental analysis, and elemental mapping studies were carried out using a scanning electron microscope (SEM) equipped with energy-dispersive spectroscopy (EDS) (FEI Quanta 200). For the SEM and EDS measurements, the samples were spotted on an aluminum sample stub. X-ray photoelectron spectroscopy (XPS) measurements were done using an ESCAprobe TPD spectrometer of Omicron Nanotechnology. Polychromatic Mg Kα was used as the X-ray source ($h\nu$ = 1253.6 eV). The samples were spotted as drop cast films on a sample stub. A constant analyzer energy of 20 eV was used for the measurements. Binding energy was calibrated with respect to C 1s at 284.8 eV. Residual fluoride concentration in water was measured (using TISAB) by a fluoride-ISE (ION 2700, Eutech Instruments). Iron concentration in water was detected using a PerkinElmer NexION 300X ICPMS (inductively coupled plasma mass spectrometry) with appropriate standards. Brunauer–Emmett–Teller (BET) surface area was measured using a Micromeritics ASAP 2020. The samples were degassed at 200 °C for 4 h under a vacuum and analyzed at 77 K with an ultrahigh pure nitrogen gas. Thermogravimetric measurements were done with a TA Instruments Q500 Thermogravimetric Analyzer (TGA) under air and N_2 atmosphere from room temperature to 900 °C, with 10 min scan rate. All the uptake capacity studies in the batch mode were done in 250 mL polypropylene conical flasks.

4. RESULTS AND DISCUSSION

4.1. Characterization of CNPFH before and after F^- Uptake. The nanocomposite has been characterized by HRTEM, powder X-ray diffraction (XRD), SEM, EDS, mapping, and TG to know about its structural features, surface and morphological properties, composition, and thermal stability. Figure 1 presents SEM images of the CNPFH nanocomposite having rough and granular surface morphology which does not change upon exposure to various F^- concentrated solutions implying that the process of interaction is adsorption. This also suggests that the composite possesses very good mechanical strength which makes it suitable for use in a water purification cartridge. The granular size is about 150 ± 50 μm. The absence of fibrillar structures confirms the complete transformation of polymeric reagents to the product. The elemental composition of CNPFH showed C, O, Fe, and N as major constituents. High carbon content is due to

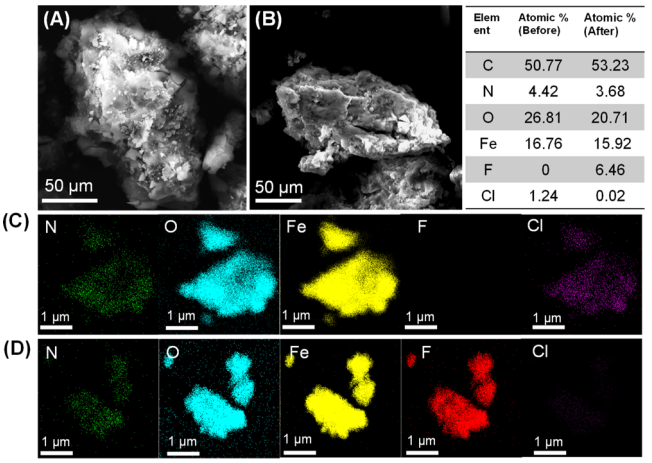

Element	Atomic % (Before)	Atomic % (After)
C	50.77	53.23
N	4.42	3.68
O	26.81	20.71
Fe	16.76	15.92
F	0	6.46
Cl	1.24	0.02

Figure 1. (A,B) show SEM of CNPFH before and after F^- adsorption, respectively. (C,D) EDS elemental mapping of N, O, Fe, F, and Cl of CNPFH before and after F^- adsorption, respectively, along with EDS quantification of elements.

nanocellulose and PANI forming the backbone of the composite structure while N and O (partly) come from the major functional groups of the respective polymers. Fe and O constitute the presence of iron oxide content in the composite. Mapping shows the uniform distribution of each element throughout the surface, specifically F^- in the adsorbed sample. Further, we note the presence of Cl which decreases in the adsorbed sample, when compared to the parent composite.

Figure 2 illustrates the HRTEM images of the CNPFH composite at a 5 nm scale where iron oxyhydroxide nanoparticles are embedded in the CNF–PANI blend matrix, confirming composite formation. The structure is largely amorphous but nanoscale polycrystalline domains appear upon beam irradiation for a few minutes, depicted by the fast Fourier transform (FFT) diffraction pattern shown in the inset (Figure 2A). Lattice planes were resolved and matched with hematite (α-Fe_2O_3) and goethite (α-FeOOH) and they appeared because of gradual conversion of metastable iron oxyhydroxide to more stable iron oxides upon beam irradiation for a few minutes. XRD spectra (Figure 2C) show characteristic broad peaks of 2-line ferrihydrite at 35 and 62° which correspond to a metastable form of iron oxyhydroxide. A weak peak at 23° corresponds to the (020) plane of PANI constituting the amorphous nanocomposite. The physical properties of the nanocomposite do not change before and after F^- removal which indicates that the process involved is adsorption. XPS survey spectra (Figure 2D) confirm the presence of C, N, O, and Fe in CNPFH before and after F^- uptake. The F^- saturated sample showed a feature for F 1s which was deconvoluted to get a clearer idea. The deconvoluted F 1s spectra (Figure 2E) show 2 peaks at 682.2 and 687.1 eV indicating two different binding sites on CNPFH for F^- adsorption. Figure 3A shows the deconvoluted C 1s peaks at 284.8, 286.5, and 288.1 eV belonging to sp^3 C–C/C–H, sp^3 C–O/sp^2 C–N, and sp^3 C–N of the parent CNPFH which has a backbone of cellulose and PANI. Figure 3C shows the Fe 2p peaks at 708.6, 711.9, and 716.3 eV because of –Fe–O–Fe–, >Fe–OH and a satellite peak. The peaks at 528.3, 529.9, and 531.2 eV in O 1s correspond to Fe–OH, Fe–O groups, and adsorbed water of parent CNPFH, respectively. They show an expected shift to 528.8, 530.4, and 531.7 eV, respectively, upon F^- adsorption. While C 1s and Fe 2p did

DOI: 10.1021/acssuschemeng.9b04822
ACS Sustainable Chem. Eng. XXXX, XXX, XXX–XXX

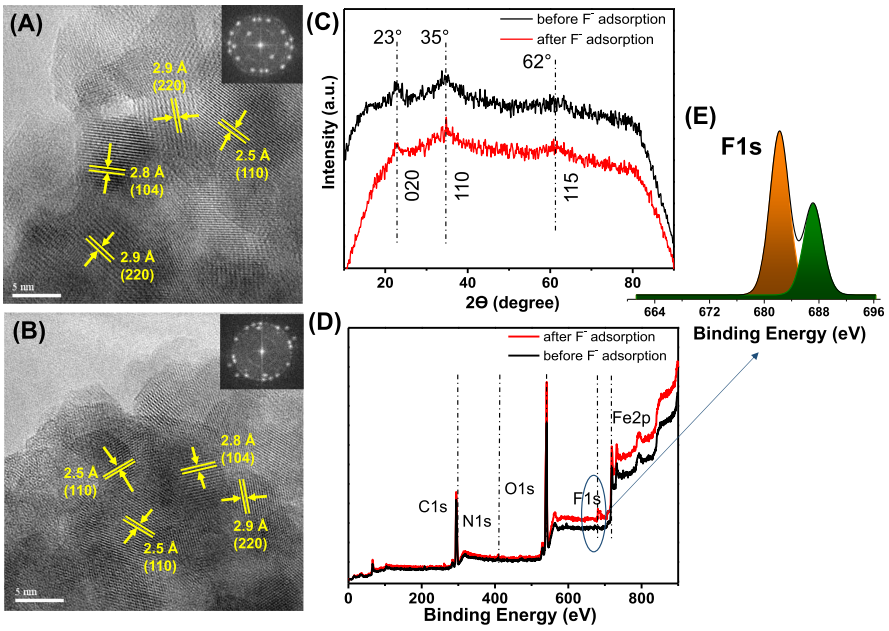

Figure 2. (A,B) HRTEM showing various crystallographic planes of CNPFH by beam-induced crystallization along with a FFT of the images before and after F^- adsorption. (C) Powder XRD patterns of CNPFH before and after F^- adsorption. (D) XPS survey spectra of CNPFH before and after F^- adsorption. Deconvoluted F 1s peaks are expanded in (E).

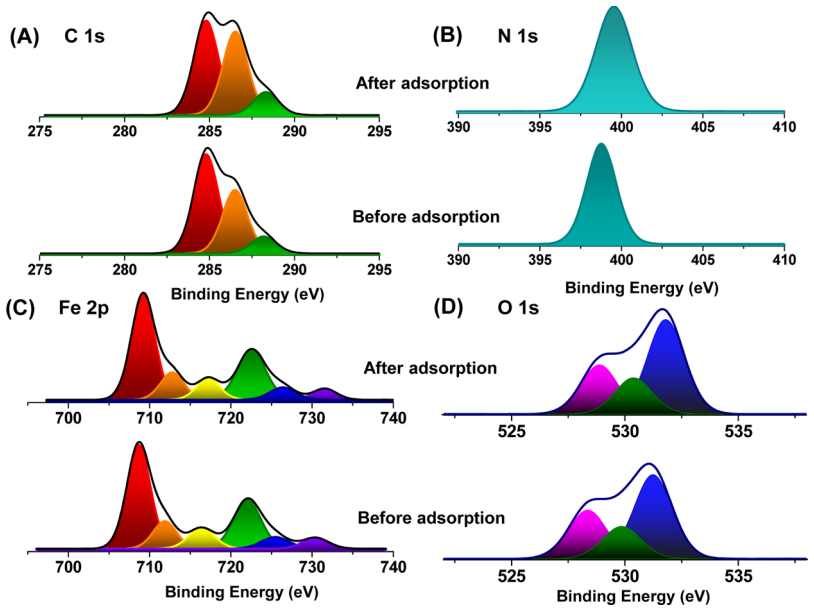

Figure 3. Deconvoluted XPS spectra of (A) C 1s, (B) N 1s, (C) Fe 2p, and (D) O 1s regions of CNPFH before and after F^- adsorption.

not show any shift in binding energy before and after adsorption, N 1s and O 1s deconvoluted peaks got shifted to higher binding energies upon F^- adsorption indicating that they bind via N− and O− sites of CNPFH (Figure 3).

To explore the mechanism of F^- adsorption in detail, we conducted an experiment where a sample of CNPFH was exposed to low F^- concentration for 5 min and the other CNPFH sample of the same weight was exposed to high F^- concentration for 3 h. This helped us understand the affinity of F^- ions toward different sites available on the composite. Figure 4A shows the F1s XPS peaks at 687.3 eV after 5 min of F^- adsorption which corresponds to F^- binding through the N^- site of PANI. Whereas, when it was left exposed to high amount of F^- for 3 h, apart from the 687.3 eV, a peak at 682.5 eV emerges which is due to F binding at the FeOOH site.[29] This has been confirmed by analyzing the F^- adsorbed cellulose−ferrihydrite composite (Figure S4) which shows a peak at 682.1 eV. Late activity of FeOOH sites may be due to the sandwiched nature of nanoparticles embedded in the PANI−cellulose blend matrix that can be reached by F^- ions, high concentrations only. Hence, N sites of PANI are better exposed at the surface than the iron oxide nanoparticles, and the former initiates the adsorption process, but the latter shows large uptake capacity. Adsorption on PANI occurs by the ion exchange mechanism where F^- replaces Cl^- which is the dopant to quaternary N of PANI leading to a peak at higher binding energy of N 1s in the adsorbed sample compared to the parent sample. Similarly, F^- was adsorbed through the ion

DOI: 10.1021/acssuschemeng.9b04822
ACS Sustainable Chem. Eng. XXXX, XXX, XXX−XXX

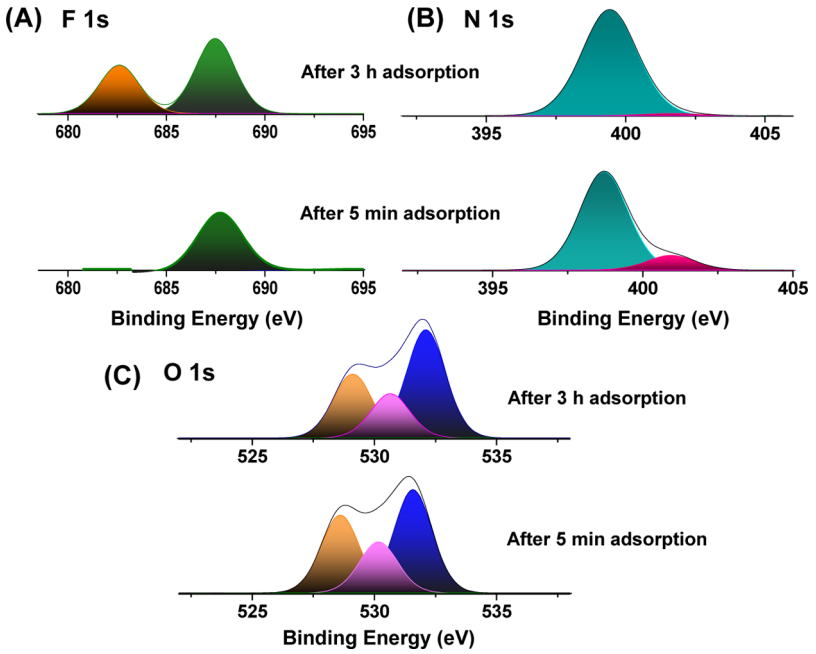

Figure 4. Deconvoluted XPS spectra of (A) F 1s, (B) N 1s, and (C) O 1s regions of CNPFH after 5 min and 3 h of F^- adsorption giving insights about the mechanism of adsorption.

exchange process with the surface hydroxyl groups of FeOOH (Figure 4C). The O 1s peaks at 530.1 and 528.6 eV corresponding to Fe−OH and Fe−O groups of parent CNPFH got shifted to 530.6 and 529.1 eV with decreased intensity for the adsorbed sample. This is supported by the Langmuir isotherm which gave a high correlation coefficient in this case (to be discussed in Figure 5).

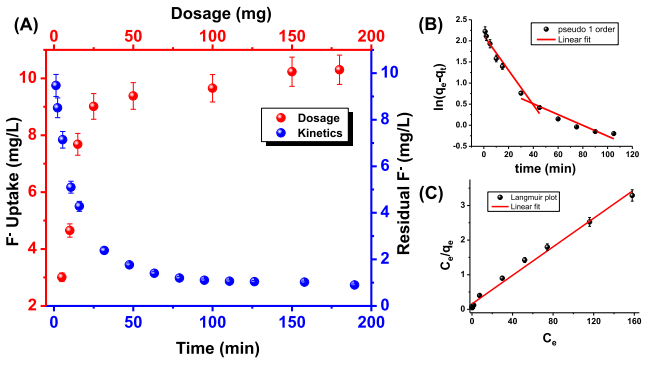

Figure 5. Batch studies for the performance of CNPFH (A) as a function of dosage and contact time, (B) pseudo first order, and (C) Langmuir isotherm model for fluoride adsorption from water.

4.2. Batch Studies of F^- Adsorption on CNPFH. It is observed that CNPFH exhibited superior performance where 50 mL of 10 mg/L F^- spiked water was treated with different dosages ranging from 5 to 180 mg, as shown in Figure 5A. About 50 mg of the composite was sufficient for bringing down the F^- concentration below 1 mg/L within 3 h of exposure time. It also shows the fast uptake kinetics of the composite where the initial 10 mg/L concentration of F^- was rapidly reduced to 1.5 mg/L within 60 min of incubation, by virtue of availability of the maximum number of free surface sites. At the end of 3 h, the residual concentration of F^- decreased further to 1 mg/L, following a relatively slower kinetics because of high surface coverage. Analyzing the kinetic data with the Lagergren's pseudo-first-order model (Figure 5B), two different slopes corresponding to F^- adsorption at two different sites belonging to PANI and FeOOH, respectively, which were in agreement with the XPS analysis of the adsorption mechanism discussed in Figure 4. Other adsorption mechanisms also are in broad agreement with the data, although they may not be strictly explainable for a two site model (Figure S1).

Figure 5C shows the linear form of the Langmuir isotherm model (eq S2) which gives a maximum adsorption capacity of 50.8 mg/g for CNPFH with a high correlation coefficient (R^2) 0.96 using eq S2. It indicates monolayer adsorption, also known as chemisorption which agrees with the ion-exchange mechanism discussed in Figure 4A.[10,39] This is further

Table 1. Comparison of CNPFH Adsorption Capacity with Other PANI/PPy-Based Adsorbents

sl no.	materials	uptake capacity (mg/g)	max wt % PANI/PPy	optimum pH	references
1	PANI	0.8	100	3	40
2	PANI/chitosan	5.5	8−10	3−4	39
3	PANI/alumina	6.6	11.6	3	24
4	FeOOH	23.8	0	7	29
5	PPy/Fe_3O_4	17.6−22.3	83	6.5	41
6	Ppy/TiO_2	33.17	9.3	7	42
7	CNF/PANI/FeOOH	50.8	14.1	3−4	this study

DOI: 10.1021/acssuschemeng.9b04822
ACS Sustainable Chem. Eng. XXXX, XXX, XXX−XXX

supported by the lower R^2 value of the Freundlich isotherm (eq S11) and a low BET surface area of 111.1 m^2/g of the composite and median pore width of 11.321 Å which do not play a major role in the adsorption process. The low surface area can be attributed to the ionic sites of the material as shown by XPS analysis, which cannot be completely picked up by N_2 adsorption, used for surface area evaluation. By using the Dubinin−Radushkevich isotherm (eq S12), we determined the E value (adsorption energy) to be 2500 kJ/mol (Figure S3). The correlation coefficient (R^2) was 0.96. The E value (>16 kJ/mol) shows chemisorption taking place in the medium. The outcome of various isotherms and kinetic parameters is summarized in Table S1. The maximum F^- uptake capacity of various other PANI/Ppy-based composites is compared with that of CNPFH, in Table 1. CNPFH shows higher removal efficiency even with lesser wt.% PANI because it exhibits synergistic performance because of simultaneous availability of FeOOH sites as well. Moreover, the adsorption of F^- on the CNPFH surface is also thermodynamically feasible and is a spontaneous process with a negative ΔG value. Using eqs S13 and S14, the thermodynamic parameters (ΔH and ΔS) with the R^2 value as 0.87 were derived. The ΔH and ΔS gave positive values which indicated that the adsorption is endothermic in nature giving rise to randomness at the solid solution interface during the adsorption of F^- species at the active sites of the composite.

4.2.1. Control Studies. The control studies were carried out by using only CNF for fluoride uptake. It showed a meager removal of 200−300 ppb of F^- out of 10 ppm which may be due to its porous structure. Hence, CNF can be considered as a platform having a high surface area which can favor blending with PANI and can embed the ferrihydrite nanoparticles in such a way that the active sites are available for adsorption of the surface of the mechanically stable composite.

CNPFH shows F^- removal more than 80% in the presence of the most interfering anions like carbonate (CO_3^{2-}), bicarbonate (HCO_3^-), nitrate (NO_3^-), silicate (SiO_3^{2-}), sulfate (SO_4^{2-}), and chloride (Cl^-) in higher concentrations, except for SO_4^{2-}, where F^- removal is about 60%. This may be because of the competing nature for both the ions to form inner-sphere complexes with functional groups at the adsorption sites. The uptake of F^- by CNPFH stays unaffected by the interfering cations like calcium (Ca^{2+}), magnesium (Mg^{2+}), potassium (K^+), and sodium (Na^+) (Figure 6A). It is able to maintain about 90% removal efficiency in a wide range of pH, that is, 3−9, but starts showing a decreased uptake when tested above pH 9 as shown in Figure 6B. This is because the decrease in surface positive charges of the adsorbent at higher pH levels (9−11) shown by zeta potential measurements, which adversely effects the coulombic interaction between the F^- ion and the adsorbent surface (Figure 6C). Also, in the presence of excess hydroxyl ions in the medium, they start competing with F^- ions for adsorption.

TGA of CNPFH in Figure 7A shows early weight loss of about 7% because of moisture below 250 °C. The weight loss of about 26% is due to the burning for carbon backbone of the cellulose and PANI polymers used in the composite between 220 and 350 °C. Next 15% weight loss is due to the loss of PANI functional groups and its dopants above 400 °C. Rest of the composite consists of iron oxide contributing 51% of the weight of the nanocomposite that stays stable till 900 °C. The iron oxide content in the composite is further studied by IR spectroscopy where Fe−O vibrations appear at 600−700 cm^{-1},

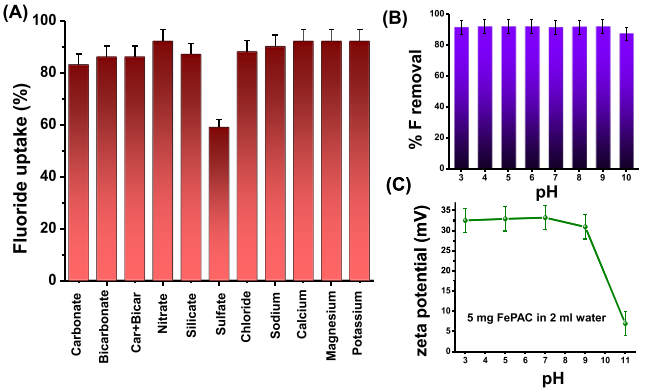

Figure 6. Batch studies for the performance of CNPFH (A) in the presence of interfering ions, (B) in the pH range of 3−10 for fluoride removal from water, and (C) zeta potential of CNPFH in the pH range of 3−11.

overlapping with a broad peak of O−H bending as shown in Figure 7B. The region between 1100 and 1600 cm^{-1} corresponds to C−O stretching of cellulose, characteristic peaks of aromatic C−N stretching, C═C, C−H, and C═N stretching of the benzenoid ring and quinoid ring that confirms the emaraldine form of PANI.[40] A band around 1570 cm^{-1} corresponding to the N−H bending of the amine salts and strong band in the 1100 cm^{-1} region corresponding to the dopant suggest the presence of the mixed (EB−ES) salt form of PANI in the nanocomposite. N−H stretching at 3378 cm^{-1} of the parent CNPFH gets broadened and shifted to 3410 cm^{-1} upon F^- adsorption.

From the perspective of environmental safety, CNPFH was tested for its leaching behavior. TOC (total organic carbon) and TN (total nitrogen) were measured of the adsorbent-soaked water. About 1.8 and 0.1 mg/L were the TOC and TN values before F^- adsorption, while 1.7 and 0.08 mg/L were the TOC and TN values of CNPFH after F^- adsorption, respectively. Iron leaching was also checked (20 and 12 μg/L before and after F^- adsorption, respectively) but all these values are below MCL (maximum contaminant levels) in drinking water, that is, 10 mg/L for TN and 300 μg/L for iron according to the United States Environmental Protection Agency (USEPA). This can be attributed to the mechanical stability imparted to the nanocomposite by the cellulose backbone. Thus, the granular material can be packed in a prototype cartridge through which contaminated water can be passed continuously in an antigravity fashion for a larger contact time without using any external energy.

4.3. Environmental Impact Assessment. This technology was assessed qualitatively and quantitatively by evaluating some of the relevant mass-based sustainability and socio-economic parameters, to determine the extent of "greenness" of the material and its manufacturing process.[43−45] The calculations were done using equations listed in an earlier paper.[46] They are also listed in the Supporting Information (eqs S4−S8) and the outcomes are summarized in Table 2.

4.3.1. Raw Materials. A major raw material includes cellulose which is renewable and biodegradable. Processing of CNFs usually involves mechanical extrusion and defibration for homogenization and chemical treatment by enzymes or strong acids and those manufacturers who use mild processing techniques for lignocellulosic fibers should be preferred for the supply of the raw material. Iron salt and aniline are used in

DOI: 10.1021/acssuschemeng.9b04822
ACS Sustainable Chem. Eng. XXXX, XXX, XXX−XXX

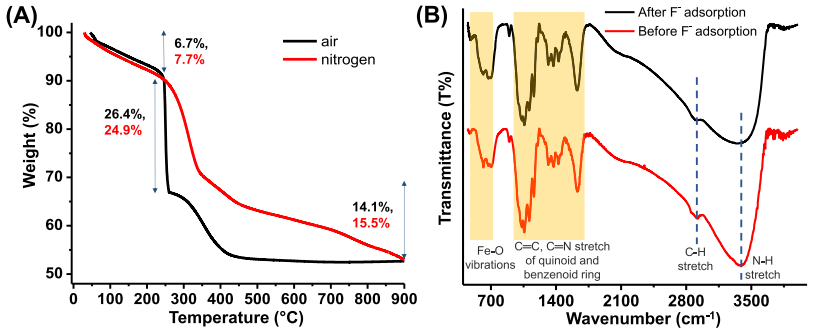

Figure 7. (A) TGA of CNPFH in an air and nitrogen atmosphere and (B) IR spectroscopy of CNPFH before and after F^- adsorption.

Table 2. Mass-Based Sustainability Metrics Evaluation for the Manufacturing Process of the CNPFH Nanocomposite

material	size (μm)	mass intensity (MI) (kg/kg)	solvent intensity (SI) (kg/kg)	reaction mass efficiency (RME) %	energy consumption (kW·h/kg)	*E*-factor
CNPFH nanocomposite	150 ± 50	1.84	38.80	54	1.78	0.6

small quantities. Water is used as the solvent. The mass intensity (excluding water) was calculated to be 1.84, while the water intensity came as 38.8. Reaction mass efficiency was 54%. Large amounts of water were used because of moderate solubility of aniline which is 3.6 g per 100 mL water at 20 °C. Reaction mass efficiency can be improved by further optimization of reactant masses and avoiding the use of excess reagents.

4.3.2. Energy Consumption. Electricity was used for operating the pH meter, stirrer, and vacuum filtration settings. The composite was dried under the sun and no electrical energy was involved in the operation of the technology. Energy intensity was calculated to be 1.78 kW·h/kg of the composite, in a lab scale synthesis set up. The energy intensity can be reduced effectively by increasing the scale of production.

4.3.3. Resulting Emissions. No harmful solvents/fumes or side products were discharged during the synthesis of the composite. Use of extra oxidants to polymerize aniline was avoided in the synthesis. The E factor (environmental factor) was calculated to be 0.6 which indicates minimum emissions. The unreacted salts coming out with wash water discharge can be removed, and water can be recycled. The method of preparation of the composite is water positive by 1−2 orders of magnitude; that is, it produces about 200 L of fluoride-free water for every 1 L of water consumed for its production.[47]

4.3.4. Toxicity Potential. As per European Chemicals Agency (ECHA), $FeCl_3$ and NaOH are classified as a skin sensitizer and corrosive, respectively, while aniline is toxic on repeated exposure to humans and aquatic life. While the first two reagents are nonflammable and stable at room temperature, aniline is in situ polymerized to PANI during composite formation and gets blended with cellulose, thereby preventing any leaching as shown by TOC analysis. PANI is not a hazardous substance or mixture according to regulation (EC) no. 1272/2008. $FeCl_3$, NaOH, and aniline show acute oral toxicity (LD_{50}) at 900 mg/kg, 280−680 and ≥102 mg/kg in mice, respectively. Therefore, the manufacturing process has to be undertaken with some simple precautionary measures.

4.3.5. Disposal of Waste. Fluoride-adsorbed composites can be subjected to multiple regenerations for subsequent adsorption cycles by suitable base treatment like NH_4OH. They can be finally disposed off in leach-free landfills.

4.3.6. Affordability. Taking 5 mg/L as the average F^- concentration in accessible water in affected communities, reagents procured at bulk industrial rates and when the same composite synthesis is optimized with the industrial grade bulk cellulose, this technology can provide fluoride-free water under $ 0.7/1000 L of clean water.

4.3.7. Social Acceptability. It depends on various criteria such as whether a technology is economical, requires low operational effort, acceptable for the users as a product, and can treat the contaminated water with the expected societal impact. The CNPFH-based technology is eco-friendly, simple, cost-effective, and does not incur excessive operational cost. The technology does not require trained manpower for implementation and maintenance. Thus, it is expected to be highly acceptable by the affected communities.

5. CONCLUSIONS

We report a green method for preparing highly efficient and sustainable cellulose/PANI-based nanocomposite and CNPFH for defluoridation of water. The 2-line ferrihydrite nanoparticles incorporated in the polymeric confinement of CNFs and doped N sites of the blended PANI function as active sites which operate synergistically for enhanced F^- removal. This also results in faster kinetics of adsorption. Therefore, the cooperation between such functional groups produce a combined performance that is greater than the sum of their separate capacities. SEM, HRTEM, XPS, and IR studies confirm that the surface, physical, and chemical properties of CNPFH remain intact even after F^- exposure till saturation. Moreover, the nanocomposite works efficiently in a wide range of pH with fast adsorption kinetics. The maximum F^- adsorption capacity of CNPFH is 50.8 mg/g which is higher than other PANI-based composites reported so far. Moreover, the robustness of the composite keeps it free from leaching, which makes it a superior option for an industrially feasible and green material for delivering affordable water in F^- affected communities worldwide. Lastly, further insights related to the environmental impact of such materials was developed by assessing relevant sustainability metrics.

DOI: 10.1021/acssuschemeng.9b04822
ACS Sustainable Chem. Eng. XXXX, XXX, XXX−XXX

■ ASSOCIATED CONTENT

Supporting Information

The Supporting Information is available free of charge at https://pubs.acs.org/doi/10.1021/acssuschemeng.9b04822.

Equations used in the main text; TEM and SEM−EDS of CNPFH before and after F^- adsorption; pseudo second-order reaction kinetic plots for the adsorption of F^-; table summarizing isotherm and kinetics parameters; Freundlich and Dubinin−Radushkevich isotherm models for F^- adsorption; XPS of F 1s for F^- adsorbed FeOOH; calculations for thermodynamic parameters related to adsorption; and physicochemical characteristics of influent natural drinking water (PDF)

■ AUTHOR INFORMATION

Corresponding Author

*E-mail: pradeep@iitm.ac.in. Phone: +91-44 2257 4208. Fax: +91-44 2257 0545/0509.

ORCID

Avijit Baidya: 0000-0001-5215-2856

Ligy Philip: 0000-0001-8838-2135

Thalappil Pradeep: 0000-0003-3174-534X

Notes

The authors declare no competing financial interest.

■ ACKNOWLEDGMENTS

The authors thank Sandeep Bose and Krithika for EDS and TOC measurements, Department of Chemistry and Department of Civil Engineering, respectively, of IIT Madras. The authors also thank the Common facility, Department of Chemistry, IIT Madras for BET and TGA measurements. The authors thank the Department of Science and Technology, Government of India and project no. DST/TM/WTI/WIC/2k17/82(G) for supporting our research program on nanomaterials.

■ REFERENCES

(1) Mukherjee, I.; Singh, U. K. *Groundwater Fluoride Contamination, Probable Release, and Containment Mechanisms: A Review on Indian Context*; Springer Netherlands, 2018; Vol. *40*.

(2) Jagtap, S.; Yenkie, M. K.; Labhsetwar, N.; Rayalu, S. Fluoride in Drinking Water and Defluoridation of Water. *Chem. Rev.* **2012**, *112*, 2454−2466.

(3) Mohapatra, M.; Anand, S.; Mishra, B. K.; Giles, D. E.; Singh, P. Review of Fluoride Removal from Drinking Water. *J. Environ. Manage.* **2009**, *91*, 67−77.

(4) Trieu, A.; Mohamed, A.; Lynch, E. Silver Diamine Fluoride versus Sodium Fluoride for Arresting Dentine Caries in Children: A Systematic Review and Meta-Analysis. *Sci. Rep.* **2019**, *9*, 2115.

(5) Jia, B.; Zong, L.; Lee, J. Y.; Lei, J.; Zhu, Y.; Xie, H.; Clemens, J. L.; Feller, M. C.; Na, Q.; Dong, J.; et al. Maternal Supplementation of Low Dose Fluoride Alleviates Adverse Perinatal Outcomes Following Exposure to Intrauterine Inflammation. *Sci. Rep.* **2019**, *9*, 2575.

(6) Ali, I. New Generation Adsorbents for Water Treatment. *Chem. Rev.* **2012**, *112*, 5073−5091.

(7) Ali, S.; Thakur, S. K.; Sarkar, A.; Shekhar, S. Worldwide Contamination of Water by Fluoride. *Environ. Chem. Lett.* **2016**, *14*, 291−315.

(8) Kheradpisheh, Z.; Mirzaei, M.; Mahvi, A. H.; Mokhtari, M.; Azizi, R.; Fallahzadeh, H.; Ehrampoush, M. H. Impact of Drinking Water Fluoride on Human Thyroid Hormones: A Case-Control Study OPEN. *Sci. Rep.* **2018**, *8*, 2674.

(9) Kimambo, V.; Bhattacharya, P.; Mtalo, F.; Mtamba, J.; Ahmad, A. Fluoride occurrence in groundwater systems at global scale and status of defluoridation—State of the art. *Groundw. Sustain. Dev.* **2019**, *9*, 100223.

(10) Maliyekkal, S. M.; Anshup; Antony, K. R.; Pradeep, T. High Yield Combustion Synthesis of Nanomagnesia and Its Application for Fluoride Removal. *Sci. Total Environ.* **2010**, *408*, 2273−2282.

(11) Jadhav, S. V.; Bringas, E.; Yadav, G. D.; Rathod, V. K.; Ortiz, I.; Marathe, K. V. Arsenic and Fluoride Contaminated Groundwaters: A Review of Current Technologies for Contaminants Removal. *J. Environ. Manage.* **2015**, *162*, 306−325.

(12) Bhatnagar, A.; Kumar, E.; Sillanpää, M. Fluoride Removal from Water by Adsorption-A Review. *Chem. Eng. J.* **2011**, *171*, 811−840.

(13) Cherukumilli, K.; Maurer, T.; Hohman, J. N.; Mehta, Y.; Gadgil, A. J. Effective Remediation of Groundwater Fluoride with Inexpensively Processed Indian Bauxite. *Environ. Sci. Technol.* **2018**, *52*, 4711−4718.

(14) Nayak, B.; Samant, A.; Patel, R.; Misra, P. K. Comprehensive Understanding of the Kinetics and Mechanism of Fluoride Removal over a Potent Nanocrystalline Hydroxyapatite Surface. *ACS Omega* **2017**, *2*, 8118−8128.

(15) Wan, S.; Lin, J.; Tao, W.; Yang, Y.; Li, Y.; He, F. Enhanced Fluoride Removal from Water by Nanoporous Biochar-Supported Magnesium Oxide. *Ind. Eng. Chem. Res.* **2019**, *58*, 9988.

(16) Cadiau, A.; Belmabkhout, Y.; Adil, K.; Bhatt, P. M.; Pillai, R. S.; Shkurenko, A.; Martineau-Corcos, C.; Maurin, G.; Eddaoudi, M. Hydrolytically Stable Fluorinated Metal-Organic Frameworks for Energy-Efficient Dehydration. *Science* **2017**, *356*, 731−735.

(17) Pistner, A. J.; Lutterman, D. A.; Ghidiu, M. J.; Ma, Y.-Z.; Rosenthal, J. Synthesis, Electrochemistry, and Photophysics of a Family of Phlorin Macrocycles That Display Cooperative Fluoride Binding. *J. Am. Chem. Soc.* **2013**, *135*, 6601.

(18) Zhao, H.; Zhao, B.; Yang, W.; Li, T. Effects of Ca^{2+} and Mg^{2+} on Defluoridation in the Electrocoagulation Process. *Environ. Sci. Technol.* **2010**, *44*, 9112−9116.

(19) Moran Ayala, L. I.; Paquet, M.; Janowska, K.; Jamard, P.; Quist-Jensen, C. A.; Bosio, G. N.; Mártire, D. O.; Fabbri, D.; Boffa, V. Water Defluoridation: Nanofiltration vs Membrane Distillation. *Ind. Eng. Chem. Res.* **2018**, *57*, 14740−14748.

(20) Pan, B.; Xu, J.; Wu, B.; Li, Z.; Liu, X. Enhanced Removal of Fluoride by Polystyrene Anion Exchanger Supported Hydrous Zirconium Oxide Nanoparticles. *Environ. Sci. Technol.* **2013**, *47*, 9347−9354.

(21) Zhang, J.; Kong, Y.; Yang, Y.; Chen, N.; Feng, C.; Huang, X.; Yu, C. Fast Capture of Fluoride by Anion-Exchange Zirconium-Graphene Hybrid Adsorbent. *Langmuir* **2019**, *35*, 6861−6869.

(22) Sreeprasad, T. S.; Maliyekkal, S. M.; Lisha, K. P.; Pradeep, T. Reduced graphene oxide-metal/metal oxide composites: Facile synthesis and application in water purification. *J. Hazard. Mater.* **2011**, *186*, 921−931.

(23) Meenakshi; Maheshwari, R. C. Fluoride in Drinking Water and Its Removal. *J. Hazard. Mater.* **2006**, *137*, 456−463.

(24) Karthikeyan, M.; Satheesh Kumar, K. K.; Elango, K. P. Conducting Polymer/Alumina Composites as Viable Adsorbents for the Removal of Fluoride Ions from Aqueous Solution. *J. Fluorine Chem.* **2009**, *130*, 894−901.

(25) Dou, X.; Zhang, Y.; Wang, H.; Wang, T.; Wang, Y. Performance of Granular Zirconium-Iron Oxide in the Removal of Fluoride from Drinking Water. *Water Res.* **2011**, *45*, 3571−3578.

(26) Chen, L.; He, B.-Y.; He, S.; Wang, T.-J.; Su, C.-L.; Jin, Y. Fe——Ti oxide nano-adsorbent synthesized by co-precipitation for fluoride removal from drinking water and its adsorption mechanism. *Powder Technol.* **2012**, *227*, 3−8.

(27) Deng, S.; Liu, H.; Zhou, W.; Huang, J.; Yu, G. Mn-Ce Oxide as a High-Capacity Adsorbent for Fluoride Removal from Water. *J. Hazard. Mater.* **2011**, *186*, 1360−1366.

(28) Kanno, C. M.; Sanders, R. L.; Flynn, S. M.; Lessard, G.; Myneni, S. C. B. Novel Apatite-Based Sorbent for Defluoridation: Synthesis and Sorption Characteristics of Nano-Micro-Crystalline

DOI: 10.1021/acssuschemeng.9b04822
ACS Sustainable Chem. Eng. XXXX, XXX, XXX−XXX

Hydroxyapatite-Coated-Limestone. *Environ. Sci. Technol.* **2014**, *48*, 5798−5807.
(29) Zhu, B.-S.; Jia, Y.; Jin, Z.; Sun, B.; Luo, T.; Kong, L.-T.; Liu, J.-H. A Facile Precipitation Synthesis of Mesoporous 2-Line Ferrihydrite with Good Fluoride Removal Properties. *RSC Adv.* **2015**, *5*, 84389−84397.
(30) Navío; Hidalgo; Colón, G.; Botta, S. G.; Litter, M. I. Preparation and Physicochemical Properties of ZrO2 and Fe/ZrO2 Prepared by a Sol−Gel Technique. *Langmuir* **2001**, *17*, 202.
(31) Sairam Sundaram, C.; Viswanathan, N.; Meenakshi, S. Fluoride Sorption by Nano-Hydroxyapatite/Chitin Composite. *J. Hazard. Mater.* **2009**, *172*, 147−151.
(32) Liao, X.-p.; Shi, B. Adsorption of Fluoride on Zirconium(IV)-Impregnated Collagen Fiber. *Environ. Sci. Technol.* **2005**, *39*, 4628.
(33) Chen, W.; Yu, H.; Lee, S.-Y.; Wei, T.; Li, J.; Fan, Z. Nanocellulose: A Promising Nanomaterial for Advanced Electrochemical Energy Storage. *Chem. Soc. Rev.* **2018**, *47*, 2837−2872.
(34) Thomas, B.; Raj, M. C.; Athira, K. B.; Rubiyah, M. H.; Joy, J.; Moores, A.; Drisko, G. L.; Sanchez, C. Nanocellulose, a Versatile Green Platform: From Biosources to Materials and Their Applications. *Chem. Rev.* **2018**, *118*, 11575−11625.
(35) Peng, B. L.; Dhar, N.; Liu, H. L.; Tam, K. C. Chemistry and Applications of Nanocrystalline Cellulose and Its Derivatives: A Nanotechnology Perspective. *Can. J. Chem. Eng.* **2011**, *89*, 1191−1206.
(36) Baker, C. O.; Huang, X.; Nelson, W.; Kaner, R. B. Polyaniline Nanofibers: Broadening Applications for Conducting Polymers. *Chem. Soc. Rev.* **2017**, *46*, 1510−1525.
(37) Kumar, A. A.; Som, A.; Longo, P.; Sudhakar, C.; Bhuin, R. G.; Gupta, S. S.; Sen, A.; Anshup, M. U.; Sankar, M. U.; Chaudhary, A.; et al. Confined Metastable 2-Line Ferrihydrite for Affordable Point-of-Use Arsenic-Free Drinking Water. *Adv. Mater.* **2017**, *29*, 1604260.
(38) MSDS—576379 https://www.sigmaaldrich.com/MSDS/MSDS/DisplayMSDSPage.do?country=IN&language=en&productNumber=576379&brand=ALDRICH&PageToGoToURL=https%3A%2F%2Fwww.sigmaaldrich.com%2Fcatalog%2Fproduct%2Faldrich%2F576379%3Flang%3Den (accessed Oct 24, 2019).
(39) Karthikeyan, M.; Kumar, K. K. S.; Elango, K. P. Batch Sorption Studies on the Removal of Fluoride Ions from Water Using Eco-Friendly Conducting Polymer/Bio-Polymer Composites. *Desalination* **2011**, *267*, 49−56.
(40) Karthikeyan, M.; Satheeshkumar, K. K.; Elango, K. P. Defluoridation of Water via Doping of Polyanilines. *J. Hazard. Mater.* **2009**, *163*, 1026−1032.
(41) Bhaumik, M.; Leswifi, T. Y.; Maity, A.; Srinivasu, V. V.; Onyango, M. S. Removal of Fluoride from Aqueous Solution by Polypyrrole/F3O4 Magnetic Nanocomposite. *J. Hazard. Mater.* **2011**, *186*, 150−159.
(42) Chen, J.; Shu, C.; Wang, N.; Feng, J.; Ma, H.; Yan, W. Adsorbent Synthesis of Polypyrrole/TiO2 for Effective Fluoride Removal from Aqueous Solution for Drinking Water Purification: Adsorbent Characterization and Adsorption Mechanism. *J. Colloid Interface Sci.* **2017**, *495*, 44−52.
(43) Sheldon, R. A. Metrics of Green Chemistry and Sustainability: Past, Present, and Future. *ACS Sustainable Chem. Eng.* **2018**, *6*, 32−48.
(44) Jiménez-González, C.; Constable, D. J. C.; Ponder, C. S. Evaluating the "Greenness" of Chemical Processes and Products in the Pharmaceutical Industry—a Green Metrics Primer. *Chem. Soc. Rev.* **2012**, *41*, 1485−1498.
(45) Starkl, M.; Anthony, J.; Aymerich, E.; Brunner, N.; Chubilleau, C.; Das, S.; Ghangrekar, M. M.; Kazmi, A. A.; Philip, L.; Singh, A. Interpreting Best Available Technologies More Flexibly: A Policy Perspective for Municipal Wastewater Management in India and Other Developing Countries. *Environ. Impact Assess. Rev.* **2018**, *71*, 132−141.
(46) Mukherjee, S.; Kumar, A. A.; Sudhakar, C.; Kumar, R.; Ahuja, T.; Mondal, B.; Srikrishnarka, P.; Philip, L.; Pradeep, T. Sustainable and Affordable Composites Built Using Microstructures Performing Better than Nanostructures for Arsenic Removal. *ACS Sustainable Chem. Eng.* **2019**, *7*, 3222−3233.
(47) Sankar, M. U.; Aigal, S.; Maliyekkal, S. M.; Chaudhary, A.; Anshup, A. A.; Kumar, A. A.; Chaudhari, K.; Pradeep, T. Biopolymer-Reinforced Synthetic Granular Nanocomposites for Affordable Point-of-Use Water Purification. *Proc. Natl. Acad. Sci. U.S.A.* **2013**, *110*, 8459−8464.

DOI: 10.1021/acssuschemeng.9b04822
ACS Sustainable Chem. Eng. XXXX, XXX, XXX−XXX